

Surface expression of thrust faulting in eastern Iran: source parameters and surface deformation of the 1978 Tabas and 1968 Ferdows earthquake sequences

Richard Walker, James Jackson and Calum Baker

Bullard Laboratories, Madingley Road, Cambridge CB3 0EZ. E-mail: rwalker@esc.cam.ac.uk

Accepted 2002 October 8. Received 2002 September 18; in original form 2002 June 14

SUMMARY

Previously unrecognised thrust faults in eastern Iran were responsible for a destructive earthquake at Tabas (1978, September 16), which produced over 80 km of distributed and discontinuous surface ruptures above a series of low anticlinal hills to the west of a major range-front. Analysis of long-period body-wave seismograms shows a simple rupture on a gently dipping ($\sim 16^\circ$) thrust, with a slight right-lateral component. This is compatible with the locally recorded aftershock distribution. Body wave analysis of two later, smaller events show similar source orientations. Several indicators of long-term active folding at Tabas can be recognised in the geomorphology, and surface ruptures from 1978 are consistent with co-seismic fold growth. Drainage incision also indicates uplift at depth on thrust faults dipping eastwards beneath the folds. Body-wave seismograms for two earthquakes near Ferdows, 150 km east of Tabas, in September 1968 also show thrust faulting at depths of ~ 10 km. Again, the surface geomorphology indicates a region of folding above an eastward-dipping thrust fault, which is ~ 10 km west of a fault bounded range-front. In both Tabas and Ferdows, the active faulting appears to show Quaternary migration away from the range-front, possibly in response to stresses produced by the elevated topography. The identification of zones of active fault-related folding is important for earthquake hazard assessment and also for an understanding of the local tectonics. We conclude that the structures which gave rise to the 1968 and 1978 earthquakes could have been recognised beforehand from the clear signals in the geomorphology, had we known what to look for at that time.

Key words: continental deformation, earthquakes, geomorphology, Iran, thrust faulting.

1 INTRODUCTION

In 1968 the town of Ferdows in eastern Iran (Fig. 1c) was badly damaged and ~ 750 people were killed by two earthquakes on the 1st (M_w 6.3) and 4th (M_w 5.5) of September. Although the surrounding area was very sparsely populated, a number of nearby villages were also damaged with a further ~ 150 deaths (Ambraseys & Melville 1982). Ten years later, on the 1978 September 16, the oasis town of Tabas, some 150 km to the west of Ferdows (Fig. 1c), was destroyed and 85 per cent of its population (~ 11 000 people) killed by an earthquake of M_s 7.4 that remains the largest instrumentally recorded earthquake in Iran. In subsequent years, four additional earthquakes have occurred near Tabas.

The faults responsible for the earthquakes had not been recognised before the earthquakes occurred, as discrete fault scarps rarely occur in the soft alluvial sediments. However, as we show below, indications of long-term, cumulative deformation are clearly visible in the geomorphology. We use seismological and geomorphologi-

cal observations to describe how the surface deformation is related to faulting at depth. From this we can better interpret the mass of complex and sometimes apparently contradictory surface ruptures that were reported, particularly for the Tabas earthquake (Berberian 1979a). At the time of the 1968 and 1978 earthquakes, the link between thrust faulting and surface folding was not much understood, nor were the surface manifestations of active folding appreciated or commonly recognised. We now know that concealed thrust faults (i.e. faults that are not directly expressed at the surface, either due to their being blind, or due to rapid erosion and sedimentation in the active region) are widespread and responsible for more recent earthquakes both within Iran (e.g. the Sefidabeh earthquake sequence in 1994; Berberian *et al.* 2000), and worldwide, such as the M_s 7.3 1980 El Asnam earthquake in Algeria (Yielding *et al.* 1981; Boudiaf *et al.* 1998) and several earthquakes in California including the 1987 Whittier Narrows (Hauksson & Jones 1989) and 1994 Northridge events (Hauksson *et al.* 1995). Understanding the geomorphological manifestations of partially or completely concealed thrust faults in seismically active regions is therefore important for identifying

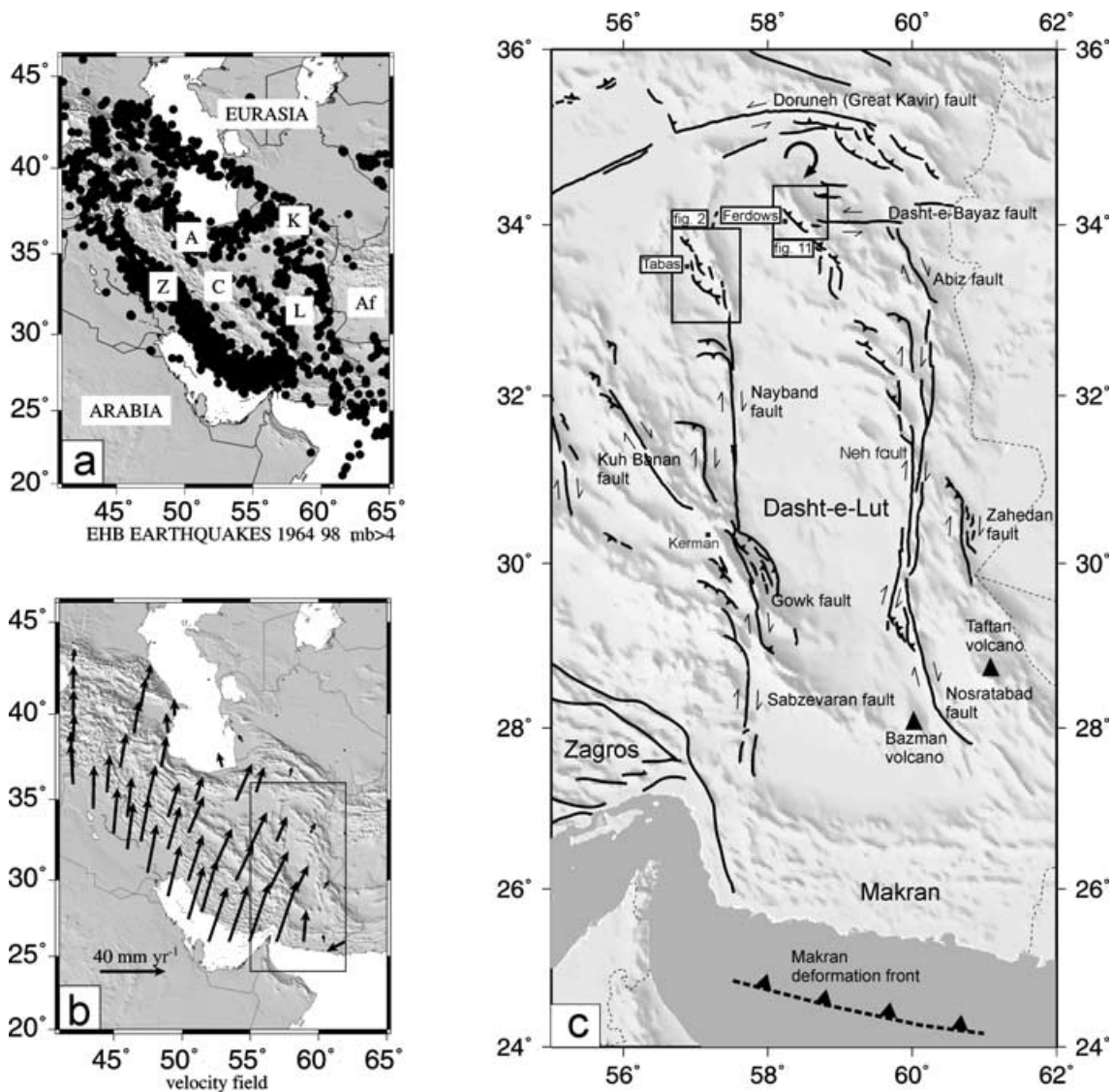


Figure 1. (a) Seismicity of Iran for the period 1964–1990. Epicentres are from Engdahl *et al.* (1998). The seismicity is mainly confined within the political borders of Iran with Eurasia and Afghanistan (Af) being essentially aseismic. Earthquake deformation within Iran is concentrated in the Zagros (Z), the Alborz (A), the Kopet Dag (K) and in eastern Iran. The aseismic central Iran and Lut blocks are denoted by C and L. (b) A velocity field for Iran estimated from the spatial variation in the style of strain rates indicated by earthquakes (from Jackson *et al.* 1995). Velocities are shown relative to stable Eurasia. Note the right-lateral shear expected along the eastern border of Iran. The boxed region shows the location of Fig 1(c). (c) Major faulting in eastern Iran. South of 34° N deformation occurs in two zones of N-S dextral strike-slip, which follow narrow mountain ranges. North of 34° N, E-W left-lateral faulting predominates. Boxes show the areas of Figs 2 and 11.

similar structures that have not had recorded earthquakes but still pose a significant seismic hazard.

2 ACTIVE TECTONICS OF EASTERN IRAN

The active deformation of Iran results from Arabia–Eurasia convergence. Shortening is mainly accommodated by distributed faulting in high mountain ranges in the south (the Zagros) and the north (the Alborz and Kopeh Dag) of the country (Fig. 1a). Surrounding regions to the north and east are aseismic and appear not to be deforming. This results in a right-lateral shear in the east of Iran as central Iran moves N–NNE relative to stable Afghanistan (Fig. 1b). South of 34° N the shear is taken up on right-lateral strike-slip faults that end in thrust faults whose displacement dies away towards their ends.

North of 34° N left-lateral strike-slip faults take up the right-lateral shear by rotating clockwise (Jackson *et al.* 1995). Again, these faults end in thrusts whose displacements die away towards their ends. This type of fault termination is a necessary consequence of strike-slip faults that do not simply link to other structures at their ends, and many examples are seen, both in Iran (Berberian *et al.* 2000) and elsewhere (e.g. Bayasgalan *et al.* 1999a; Meyer *et al.* 1998). The 1968 Ferdows and 1978 Tabas earthquakes both occurred on thrust fault systems of this type.

3 TABAS

3.1 Topography and Geology

Fig. 2 shows the major elements of the Tabas region. The Tabas fold system is visible in the alluvial apron between the Tabas playa

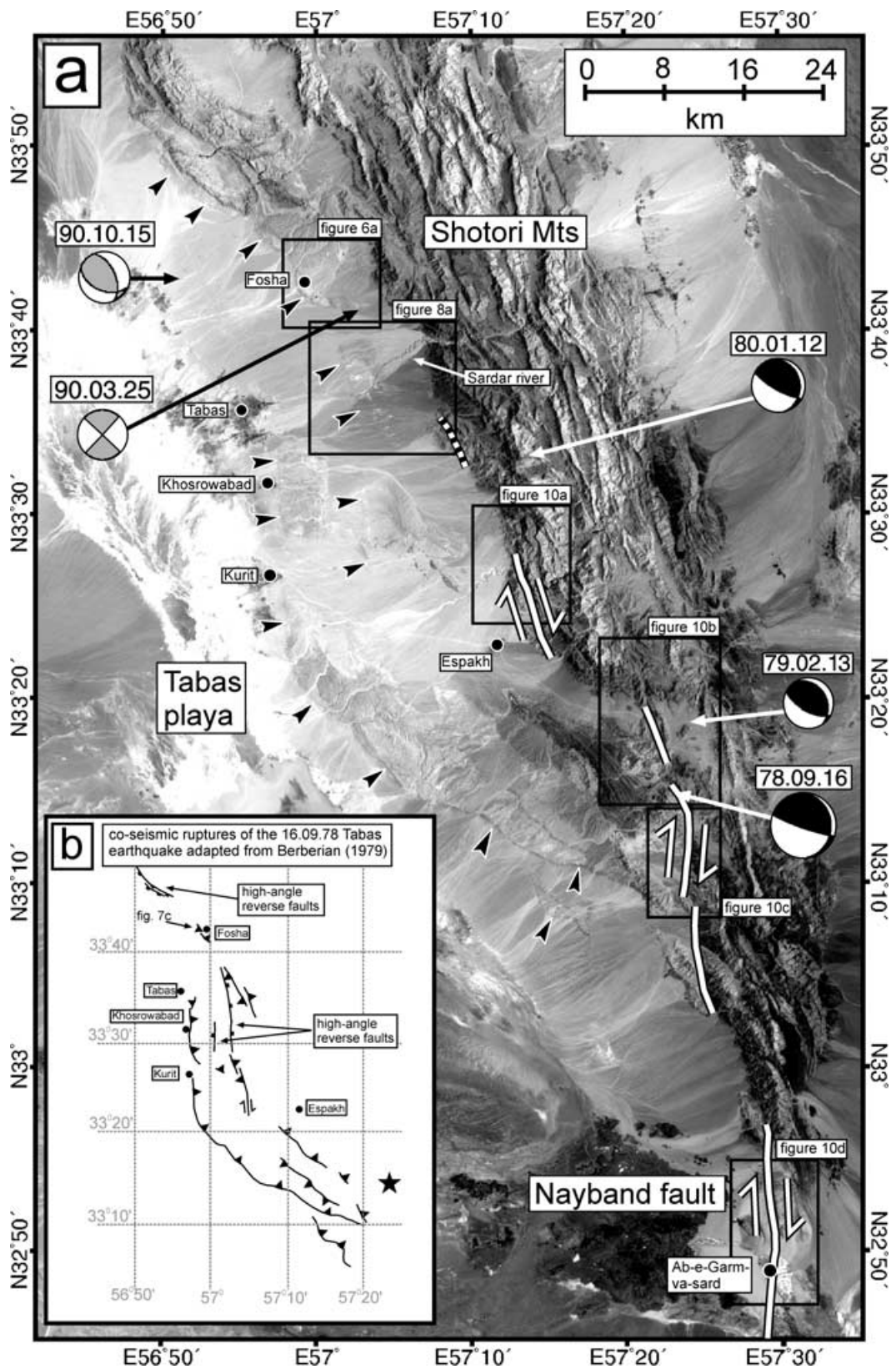


Figure 2. (a) LANDSAT TM image of the Tabas region. Tabas lies between the high Shotori mountains to the east and the Tabas playa to the west. The fold segments adjacent to Fosha, Khosrowabad and the Sardar river are discussed in the text. A discontinuous zone of strike-slip faulting is identified in the western Shotori mountains (white lines). Fault plane solutions for five events are shown (black for events modelled in this study, grey for those from the Harvard CMT catalogue). Epicentres are from the catalogue of Engdahl *et al.* (1998) and may be in error by up to 15 km. Boxes show locations of later figures. (b) Simplified ruptures from the 1978 earthquake (after Berberian *et al.* 1979) are shown in black. High-angle faults have ticks on the upthrown sides. The black star is the 1978 main shock epicentre from Engdahl *et al.* (1998).

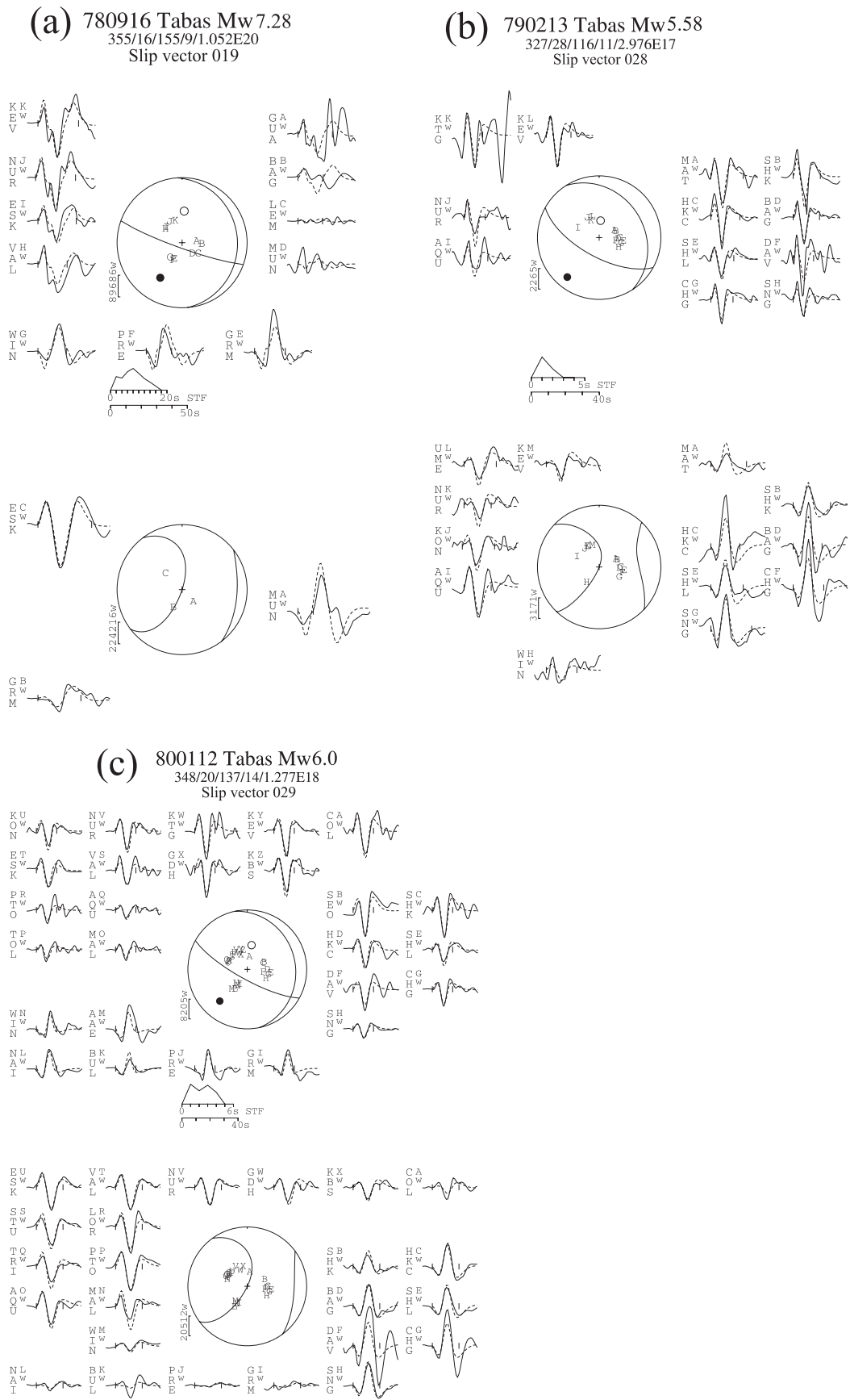


Figure 3. Final inversion results for (a) the 1978 September 16 Tabas main shock (b) the 1979 February 13 event and (c) the 1980 January 12 event.

Table 1. Source parameters of the 1978 September 16 Tabas main shock. SV is the slip vector azimuth, assuming that the east-dipping nodal plane is the fault plane. The source parameters in each case are determined by different methods that are described in the final column.

Source	Strike	Dip	Rake	SV	Depth	M_o ($\times 10^{20}$)	M_w	Method
This paper	355	16	155	19	9	1.052	7.28	Body-wave inversion
Berberian <i>et al.</i> (1979)	332	31	110	36	–	–	–	First motions
Harvard CMT	328	33	107	38	11	1.32	7.4	Centroid moment tensor
Niazi & Kanamori (1981)	330	30	110	36	–	1.5	7.4	Surface wave moment
	–	–	–	–	–	0.82	–	<i>P</i> -wave moment
Silver & Jordan (1983)	–	–	–	–	–	1.3	–	Total moment spectra

depression (~ 600 m above sea level) and the Shotori mountains. The NNW–SSE Shotori mountains form the highest topography (~ 2900 m). The relief of these mountains is in contrast to the low rounded hills of the Tabas fold system, which do not rise more than ~ 100 m above the surrounding gravel apron. The Shotori mountains are composed of heavily deformed Palaeozoic and Mesozoic rocks. Changes in sediment thickness from the Shotori mountains towards Tabas indicate several periods of fault reactivation since the late Pre-Cambrian (Stöcklin *et al.* 1965; Berberian 1979a), with a final phase of shortening in the Late Tertiary. West of the Shotori mountains, deposition is typified by Neogene marls overlain by conglomerate. The marls are exposed in the cores of the Tabas anticlines and produce light shades in LANDSAT imagery (Fig. 2). River terraces and laterally equivalent gravel fans are widespread within both the Shotori mountains and the Tabas folds. These are probably Quaternary surfaces (Stöcklin *et al.* 1965) and are often deeply incised.

3.2 Seismicity of the Tabas fault system

We first obtain source parameters for the 1978 main shock as well as for additional earthquakes on 1979.02.13 and 1980.01.12 by modelling *P* and *SH* body waves. Two other events in 1990 in the northern part of the system were too small for their waveforms to be modelled with our technique, but CMT solutions are available from the Harvard catalogue (Fig. 2). Our results indicate that the 1978 main-shock occurred on a gently dipping thrust and that much of the main fault slip at depth may not have reached the surface. We then compare these results with co-seismic ruptures mapped in 1978.

3.2.1 Source parameters of the 1978 September 16 earthquake

The teleseismically-relocated epicentre for the main Tabas shock is at 33.25° N, 57.38° E (Engdahl *et al.* 1998), placing the shock within the southern Shotori mountains (Fig. 2). This location may be in error by 10 to 15 km, which is typical for large earthquakes in Iran after 1970 (Berberian 1979b), but even with this error, it is near the southern end of the rupture sequence (Fig. 2b), implying a northward rupture propagation. Although there is no proof of this

in our body wave inversion, analysis of strong motion records also support a northward propagation (Shoja-Taheri & Anderson 1988).

We used body waveforms to constrain the earthquake source parameters. Paper seismogram records for stations of the WWSSN network in the epicentral range of 30 – 90° were digitised. We then used the MT5 version (Zwick *et al.* 1995) of McCaffrey & Abers (1988) and McCaffrey *et al.* (1991) algorithm, which inverts the *P* and *SH* waveform data to obtain the strike, dip, rake, centroid depth, seismic moment and source time function. We always constrained the source to be a double-couple. The method and approach we used are described in detail elsewhere (e.g. Nabelek 1984; Taymaz *et al.* 1991) and are now too routine to justify repetition here.

The result of our inversion for the main shock is shown on Table 1 along with other published source parameters. Fault plane solutions for all three of the earthquakes are shown in Fig. 3 and the source parameters for all the earthquakes determined by body-wave inversion are summarized in Table 2. The source parameters determined for the main shock (Fig. 3a) and the two later earthquakes (Fig. 3b–c) all have similar mechanisms that involve predominantly thrust faulting on shallow planes dipping between 16° and 28° to the east (Table 2). Relatively few seismograms are available for the main shock as many were off scale. The strike of the fault plane in the main shock is not well constrained, but all three earthquakes have a well constrained steep nodal plane which requires the slip vectors to be similar in each case, assuming that the actual fault plane dips NE beneath the Shotori mountains for each one (Table 2). In particular, our solution for the 1980.01.12 event, which, like the main shock, has a steep SW-dipping nodal plane, is not sensitive to changes in strike of the fault plane, as changes in strike are balanced by a direct trade-off with rake, without the need to change the well constrained steep nodal plane. But, the strike of the fault plane must be approximately NW–SE because of the topography and structure at the surface (Fig. 2), this means that the dip of the fault plane is constrained to within $\pm 5^\circ$, as changing the dip affects seismograms at stations close to the *P* and *SH* nodal planes, resulting in a degradation in the visual fit of synthetic seismograms. This, and the similarity between all three solutions (Fig. 3) increases our confidence in the relatively poorly constrained main shock mechanism. The component of right-lateral strike-slip indicated by the slip vectors in all three earthquakes is also seen in the co-seismic ruptures, which we address later.

Table 2. *P* and *SH* body-wave inversion results for the Tabas and Ferdows earthquake sequences. Epicentres are from Engdahl *et al.* (1998).

Event	Lat.	Long.	Strike	Dip	Rake	SV	Depth	M_o ($\times 10^{18}$)	M_w
1968 Sept. 01	34.07	58.21	307	37	95	32	10	2.959	6.25
1968 Sept. 04	34.03	58.31	340	34	100	58	9	0.2163	5.49
1978 Sept. 16	33.25	57.38	355	16	155	19	9	105.2	7.28
1979 Feb. 13	33.31	57.40	327	28	116	28	11	0.2976	5.58
1980 Jan. 12	33.55	57.23	348	20	137	29	14	1.277	6.0

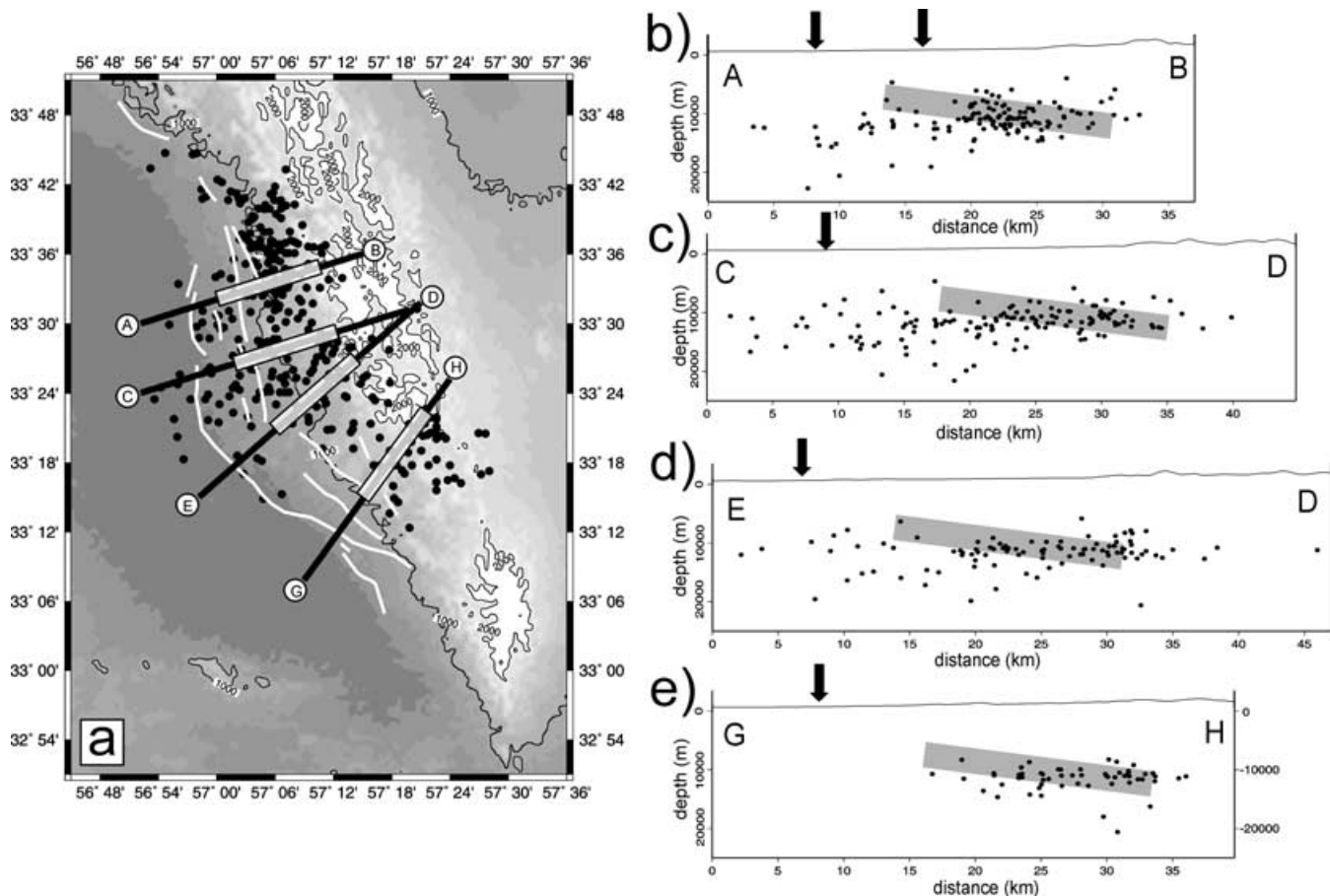


Figure 4. GTOPO30 topography of the Tabas region with aftershock locations from Berberian (1982) and co-seismic ruptures after Berberian (1979a). Lines correspond to the sections shown to the right. (b-e) Cross-sections through the Tabas thrust system. Lines of section are shown on Fig. 4(a). Aftershocks up to 10 km from the line of section are projected. Black arrows above the sections mark the positions of co-seismic ruptures at the surface. The main rupture surface determined from inversion of body-waves (see text) is represented by the grey bar. The centre-point is fixed by the centroid depth of 9 km. As the epicentral location is expected to vary by ~ 10 km, the lateral position of the main rupture is located by eye to overlie the most dense aftershock activity.

As both the co-seismic ruptures and longer-term folding occur in discrete segments (see Fig. 2), discrete earthquake sub-events might be expected. Analysis of strong motion records certainly supports this, and at least four sub-events are recognised, propagating from south to north (Shoja-Taheri & Anderson 1988). However, relative locations of the sub-events are not well enough resolved to associate them with particular fold segments at the surface. The source time function obtained from our long-period inversion indicates a single, simple rupture event at these lower frequencies lasting for 18 s. With a rupture velocity of ~ 3.5 km s^{-1} , this gives a 65 km fault length, which is close to the observed 80 km length of the co-seismic ruptures described by Berberian (1979a). In any case, the 80 km rupture length may contain the effects of aftershocks as well as the main shock. We therefore consider the earthquake as a single continuous event without the need to invoke a complicated composite event. Therefore, although it is probable that the fault is segmented at depth (as reflected by the strong motion records and possibly by the surface folding as well), we do not attempt to model this.

We can also attempt to compare the main shock source parameters determined in this study with aftershocks recorded for a period of 30 d afterwards by Berberian (1982), shown in Fig. 4(a). We first assume that the ratio of average slip to rupture length (\bar{u}/L) is 5×10^{-2} , which is typical for intraplate earthquakes (Scholz 1982). We can then use the seismic moment and a rupture length of 65 km

(determined by multiplying the main shock source time function duration of 18 sec (Fig. 3a) by a rupture velocity of 3.5 km s^{-1}), to estimate a down-dip fault width of ~ 17 km and an average slip of ~ 3.3 m. The rupture surface is then represented as a grey bar on cross-sections perpendicular to the trend of the surface deformation (Fig. 4b-e). The centre point of the bar is consistent with our determination of centroid depth (Fig. 3a and Table 1), but the depth is not well constrained by the waveform modelling because of a trade-off with source time-function duration, which is common for dip slip earthquakes of this magnitude. With this consideration, and because the instrumental epicentre location may be in error by ~ 10 km (Berberian 1979b), we placed the bar by eye to overlie the densest aftershock activity. The location of these bars are shown in plan view on Fig. 4(a). Most of the aftershocks occur in a near-horizontal band that is close to the gently eastward-dipping plane we assume ruptured in the main shock. These observations, and the relatively small co-seismic displacements seen at the surface (Berberian *et al.* 1979, see below), imply that most of the fault slip at depth failed to reach the surface.

3.2.2 Coseismic surface ruptures of the 1978 September 16 earthquake

Co-seismic ruptures were mapped in detail by Berberian (1979a). Discontinuous surface ruptures in ten main segments extended

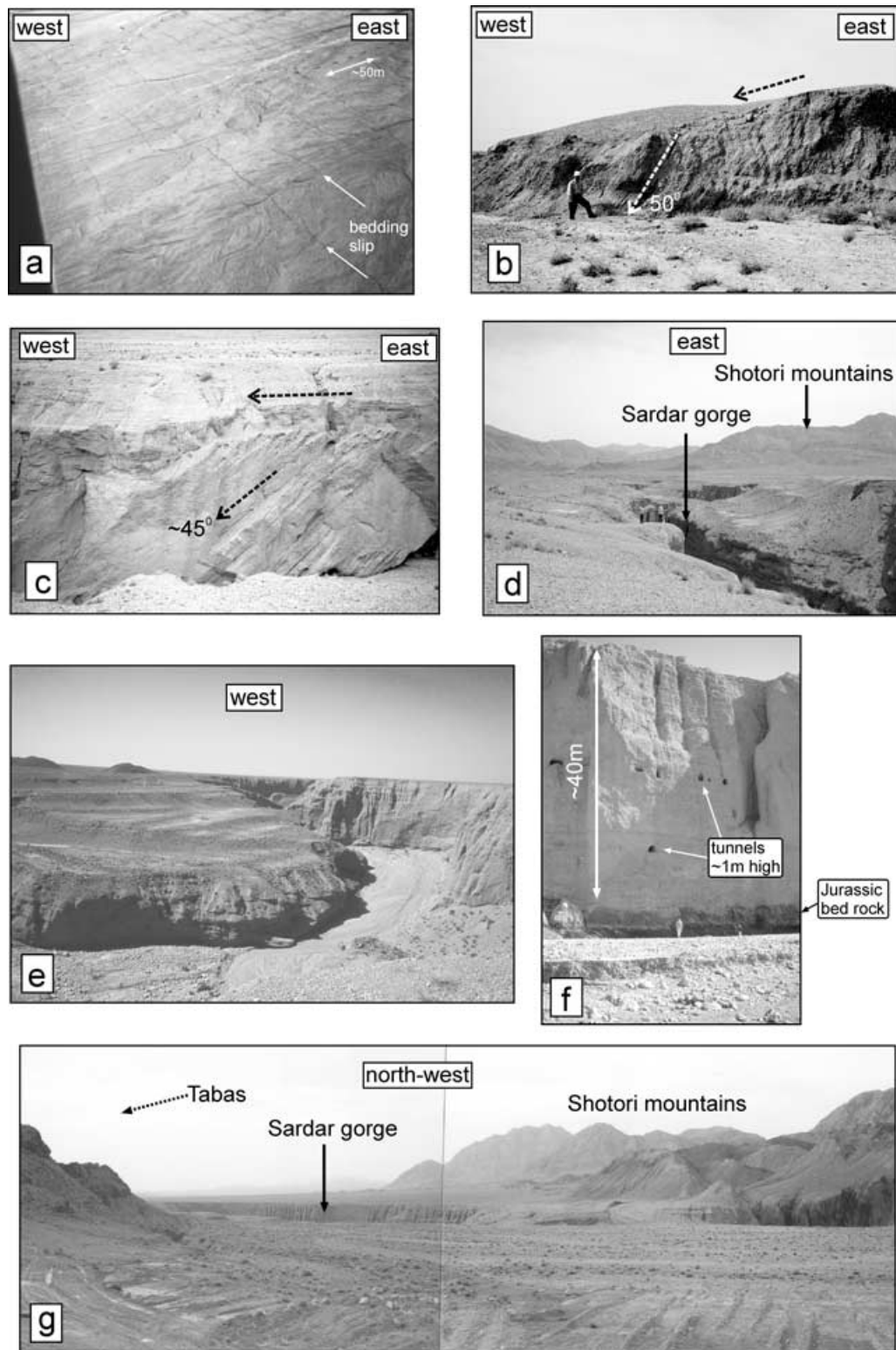


Figure 5. Extensive bedding slip developed south of Tabas in the 1978 earthquake. Distance between Qanat tunnels is ~ 20 m (photograph courtesy of M. Berberian). (b) Gravels exposed in the north face of a river cutting ~ 2 km north of Khosrowabad ($33^{\circ} 33' .36N$ $56^{\circ} 57' .50E$). Unconformable relationships between underlying (steeper) and overlying (gently) dipping gravels are seen. (c) Unconformable relationship between steep underlying gravels and gently-dipping overlying gravels in the north face of the Sardar river canyon near $33^{\circ} 36' .50N$ $57^{\circ} 02' .50E$ near the western flank of the fold. (d) Looking east from eastern margin of the Sardar fold near $33^{\circ} 38' .50N$ $57^{\circ} 04' .75E$. Incision of the Sardar river into abandoned gravel fan deposits (several terraces can be seen in the southern wall of the canyon). (e) Staircase terracing in incised meanders of the Sardar river, view looking west from near $33^{\circ} 39' .65N$ $57^{\circ} 07' .00E$. (f) Incised terrace of the Sardar river within the Shotori mountains. Jurassic bedrock is exposed at the base of the gravels. (g) The Sardar canyon as it enters the Shotori mountains at $33^{\circ} 39' .40N$ $57^{\circ} 07' .30E$. The abandoned alluvial surface is not offset by faulting at the mountain edge, which therefore must have been quiescent at least since deposition of the fan.

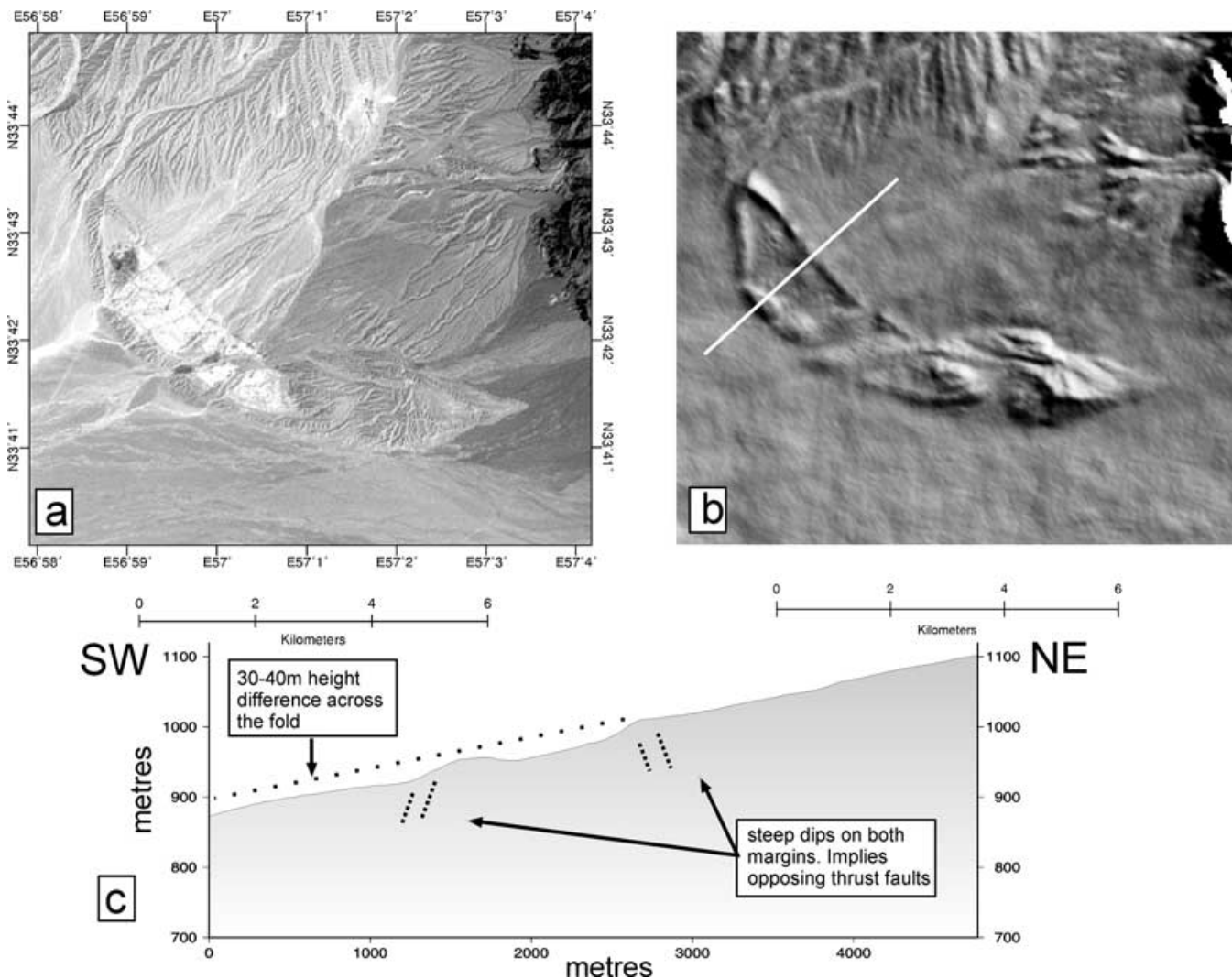


Figure 6. ASTER image of the Fosha fold segment (see Fig. 2, for location). The folding is very clear, as is the asymmetry of drainage incision, which is seen only to the east of the fold. (b) 40 m resolution digital elevation model of the Fosha segment of the Tabas system. The white line represents the line of section in Fig. 6(c). (c) Section through the 40 m DEM across the Fosha fold. Steep dips at both margins of the fold suggest both margins are underlain by opposing thrust faults. Alluvial surfaces differ in height across the fold by ~40 m.

along a NNW–SSE trend for ~85 km. They closely followed the low hills of the Tabas fold system. Shallow-dipping thrust ruptures formed along the western margins of these folds (Fig. 2b). The maximum displacement across these ruptures was ~35 cm (Berberian 1979a), which is significantly less than the ~3.3 m of slip expected along the main rupture plane using the assumed ratio of average slip to rupture length introduced earlier (Scholz 1982).

Ruptures also developed within the folds. These had steeper dips, and were interpreted as reverse faults with steep to vertical dip (Berberian 1979a), see Fig. 2b. However we suspect that some of these were surficial normal faults, or near-vertical fissures within the core of the folds, as seen at El Asnam in 1980 (Yielding *et al.* 1981). Significant internal deformation also occurred within the folded Neogene deposits in the hanging walls of the observed thrust faults, with extensive bedding plane slip over an ~8 km wide zone. This bedding plane slip was most dramatically demonstrated across dry river beds, where it was clearly developed in extensive fluvial surfaces (Fig. 5a). A right-lateral component was noted in several localities (Berberian 1979a).

The seismology suggests that at least the distributed surface ruptures within the folds were not part of the main seismogenic surface responsible for the Tabas earthquake, which probably involved ~3.3 m of slip on a gently eastward dipping plane. Thrust ruptures along the western margins of the folds may be the tips of the main rupture reaching to the surface, but the small displacements across them (~35 cm) indicate that much of the slip at depth did not reach the surface at all. We suggest that the suite of surface ruptures is predominantly due to co-seismic fold growth that accommodates the major part of the thrust movement at depth.

3.3 Geomorphological expression of thrust faulting at Tabas

The geomorphology of active fault zones often contains information on the long-term development and evolution of the faulting, which is impossible to obtain using seismology alone (e.g. Burbank *et al.* 1996; Jackson *et al.* 1996; Keller *et al.* 1998; Oskin *et al.* 2000). In the following section we use simple observations of the

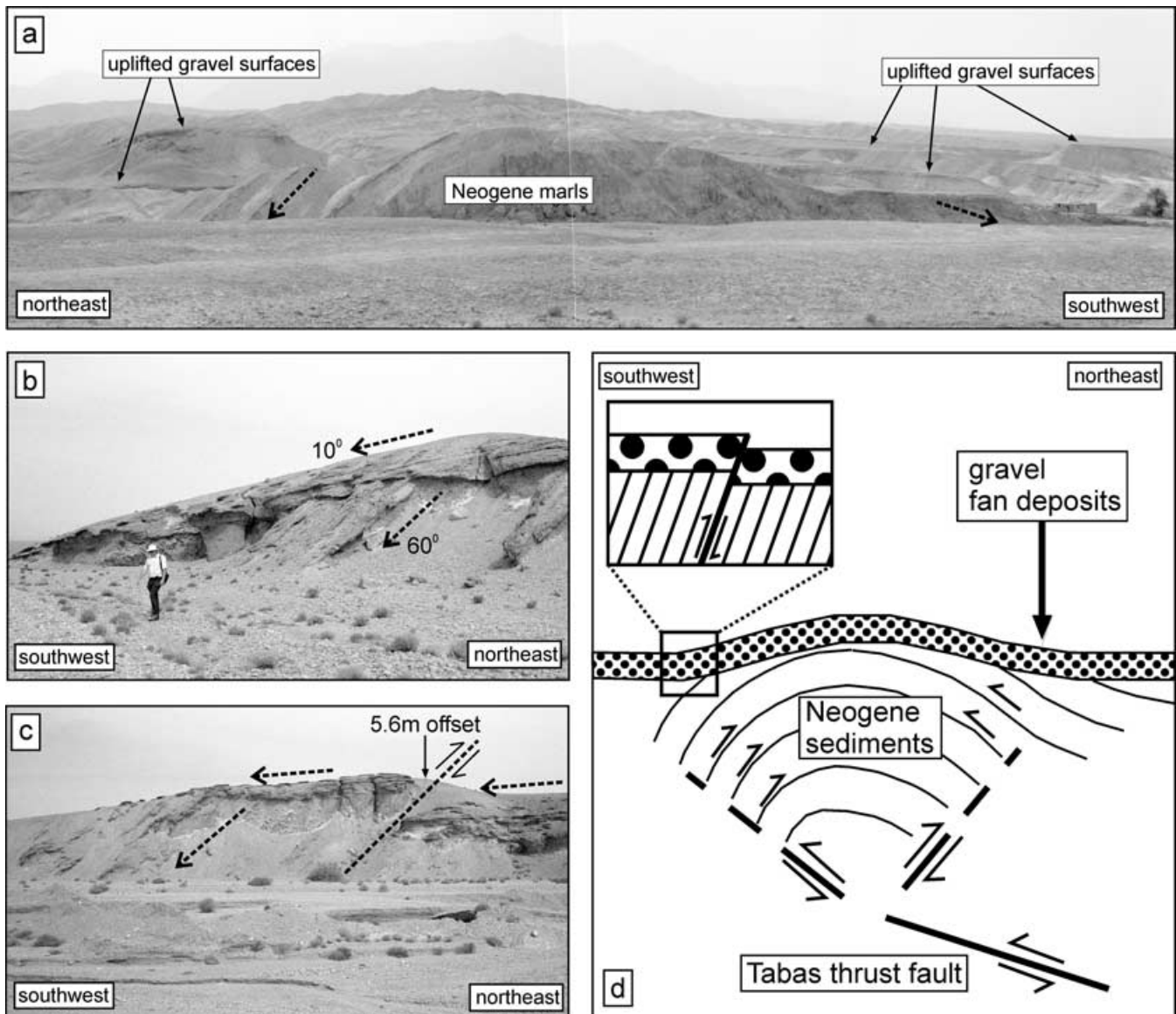


Figure 7. Indicators of long-term and co-seismic growth on the Foshā fold segment (see Fig. 6, for location). (a) Photograph looking SE from $33^{\circ} 42' .01N$ $57^{\circ} 00' .03E$. Two uplifted and tilted gravel surfaces are seen. These lie unconformably on strongly tilted Neogene marl beds. House and palm trees at right for scale. (b) Photograph looking NW along the nose of the Foshā fold, exposed in a river cutting ($33^{\circ} 41' .69N$ $56^{\circ} 59' .42E$). The unconformity between younger and older gravels can be seen. We are standing on a recent and still active river terrace. (c) Westward dipping thrust fault developed in young gravels on the western margin of the fold ($33^{\circ} 42' .32N$ $56^{\circ} 58' .78E$). The orientation of the thrust matches the dip of underlying, tilted Neogene marls. (d) Cartoon showing how the folding at Foshā grows by flexural slip between beds. Continual reworking of folded alluvial gravels into new, un-tilted surfaces results in unconformities between younger and older beds. Slip on steep underlying beds displaces younger gravels forming small thrust faults (as seen in Fig. 7c).

geomorphology to show long-term folding at Tabas. Furthermore, from the landscape, we can infer the presence of an eastward dipping thrust fault at depth below the Tabas folds.

3.3.1 Long-term folding

Fig. 6(a–b) shows the Foshā segment of the Tabas fold system (see Fig. 2, for location). The folding is clearly visible in digital topography and ASTER satellite imagery. The Foshā fold is ~ 2 km wide and ~ 5 km long. It is developed in alluvial deposits shed from the Shotori mountains and folded Neogene marls are exposed in the core of the fold (which show as light-shaded regions on the ASTER image). There are several key observations that point towards long-term folding and uplift.

First, remnants of gently tilted alluvial and fluvial gravel surfaces are preserved at heights of 10 to 20 m above the present-day river levels (Fig. 7a). This implies either fold uplift of this amount since the gravel surface was deposited or the same amount of lowering of the fluvial base-level. As these uplifted gravels are preserved within the folded region and stop sharply at the western margin of the fold, it seems likely that their presence records uplift of the fold with respect to local base-level (e.g. Bullard & Lettis 1993; Burbank *et al.* 1996). Furthermore, the uplifted gravels lie unconformably on older, steeper Neogene marls (Fig. 7a). Unconformable contacts between older and younger gravels can be seen in the wall of a river cutting the western flank of the fold (Fig. 7b). This is a direct indication of long-term growth of the fold, with fluvial and alluvial gravels repeatedly going through a process of folding, erosion

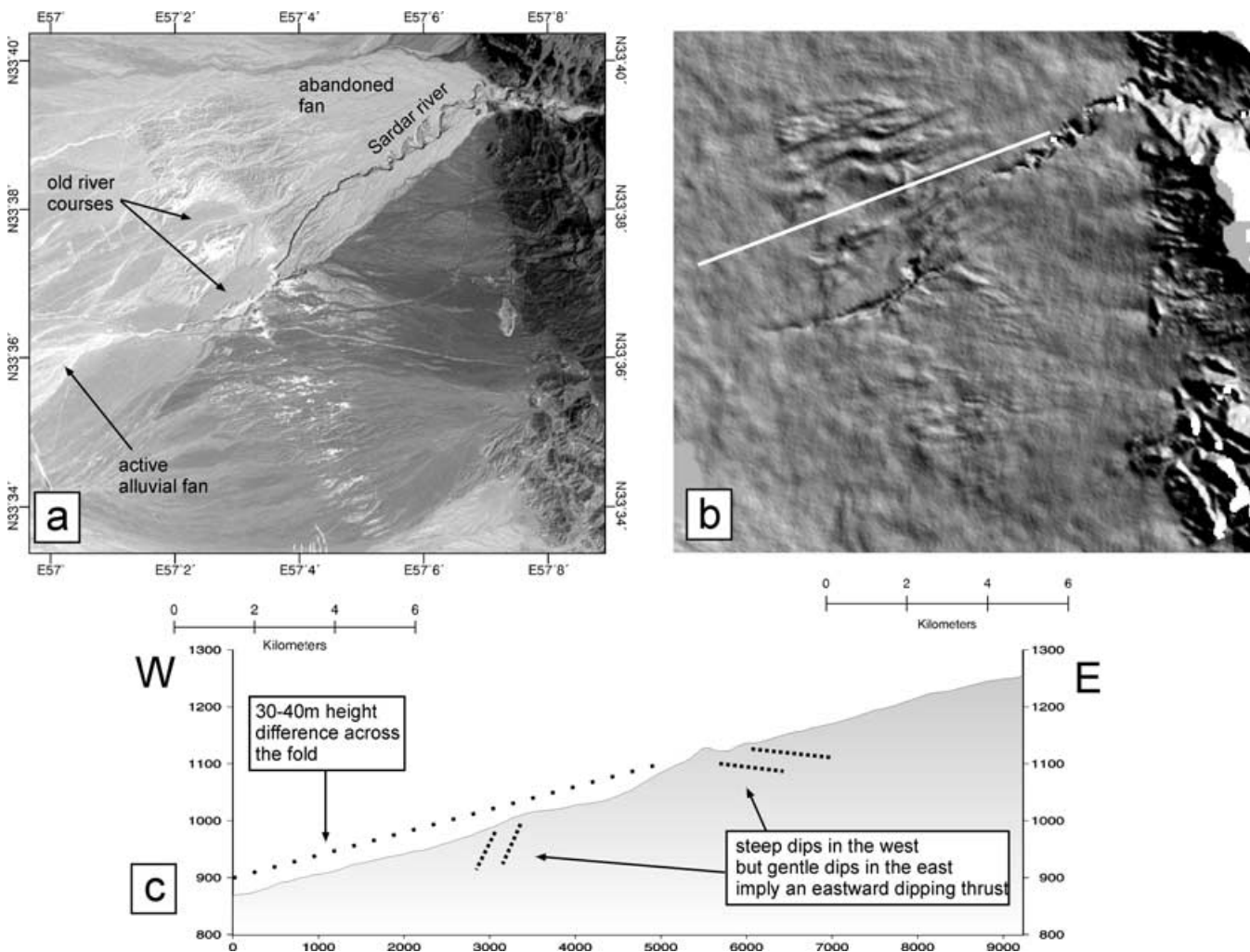


Figure 8. (a) ASTER image of the Sardar fold segment (see Fig. 2, for location). The fold forms an ~ 4 km wide zone of uplifted and incised alluvium trending NNW through the centre of the image. The Sardar river has cut an ~ 100 m deep gorge to the east of the fold. At the western margin of the fold, the Sardar river forms an active alluvial fan. (b) 40 m resolution digital elevation model of the Sardar segment of the Tabas system. The white line represents the line of section in Fig. 6(c). (c) Section through the 40 m DEM across the Foshia fold. Steep dips are only found in the western margin of the fold, implying a westward vergence. Alluvial surfaces differ in height across the fold by ~ 40 m. The line of section roughly follows a single alluvial surface, abandoned since the Sardar river cut into it, which is continuous through the fold in old river courses.

and redeposition as new gravel surfaces are in turn uplifted and folded, as depicted in Fig. 7(d). Similar relationships are also found in the western flanks of the Sardar and Khosrowabad fold segments (Fig. 5c–d). The folding and uplift is accommodated by bedding-plane slip between steeply dipping beds, as observed in 1978 (Berberian 1979a). Similar long-term fold growth is seen in the northern Tien Shan (Avouac *et al.* 1993), and in New Zealand (Lamb & Vella 1987). At Foshia, Berberian (1979a) recorded a westward dipping thrust fault with cumulative slip of 5.6 m, which moved by 7 cm in 1978 (Fig. 7c). This was one of many surface ruptures activated in 1978 that showed dips apparently inconsistent with the source parameters determined from seismological investigation (see Fig. 2b). However, the dip of this minor fault is close to that of the steeply dipping folded Neogene deposits that underlie the gravel surfaces, and it is probable that the fault represents repeated bedding-plane slip within the Neogene sediments, with the 5.6 m of offset accumulating through slip in many earthquakes (Fig. 7d). Although our arguments are based on the northern part of the Tabas system, where access in the field is possible, similar relationships are seen throughout the fold system.

Bedding-slip might not have caused all of the high-angle co-seismic ruptures that were recorded within the folds (see Fig. 2). Some of these were interpreted as steep splay faults that link with a gently dipping master fault at depth (Berberian 1979a). However, it now seems likely that many were superficial structures related to fold growth and that at least some were probably normal faults accommodating extension above growing anticlines. There are many examples in which co-seismic folding is accommodated by normal faulting along the fold axis, such as at Sefidabeh in eastern Iran (Berberian *et al.* 2000), the Gobi-Altay of Mongolia (Bayasgalan *et al.* 1999b) and El Asnam in Algeria (Yielding *et al.* 1981).

3.3.2 Geomorphic evidence for thrust faulting at depth

The results from seismology and the locations and types of co-seismic rupturing indicate that the surface folding is linked to fault movements at depth. Several of the folds (e.g. the Foshia and Khosrowabad segments, see Fig. 2) have steeply dipping beds at both their western and eastern margins (also reflected in co-seismic ruptures, see Fig. 2b), presumably indicating opposing reverse faults beneath

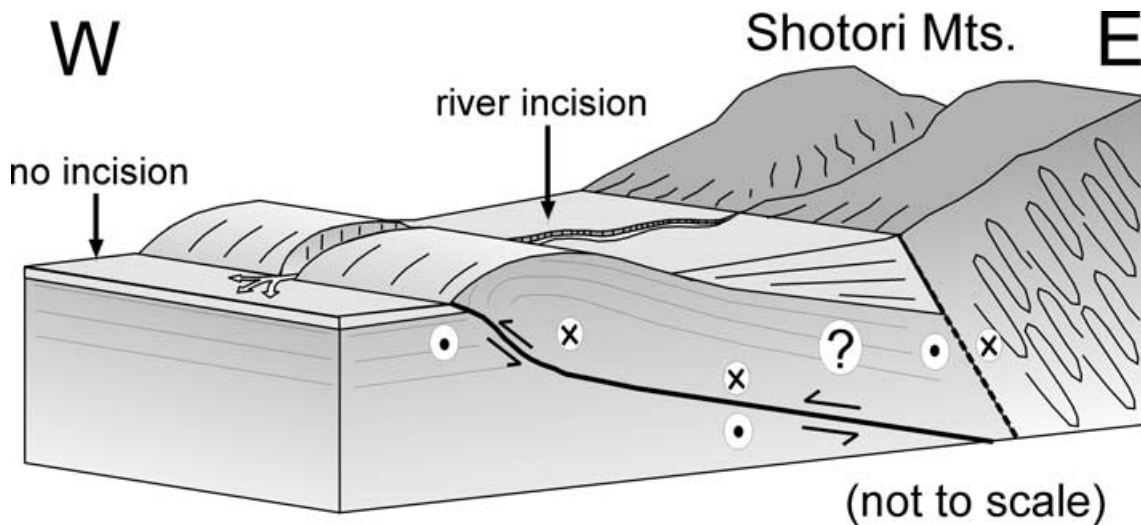


Figure 9. Cartoon cross-section through the Sardar fold segment. Surface folding has a wavelength of ~ 4 km, relating to the depth at which the underlying thrust steepens toward the surface. Widespread drainage incision east of the fold implies uplift on a gently eastward-dipping thrust at depth (which is consistent with seismological results, see Figs 3 and 4). Thrust faulting at the edge of the Shotori mountains appears to be inactive at the surface and does not displace alluvial gravels, although strike-slip faulting is seen to the south of the Sardar river along the mountain range front (Figs 2a and 10). A strike-slip component within the folds is indicated by seismology and surface ruptures. Other folds in the Tabas system show slight variation from this cartoon. Several segments (e.g. Fosha and Khosrowabad) appear to have both frontal and back-thrusts. Also, the asymmetric drainage incision is less clear in the westernmost folds (e.g. Khosrowabad), and might imply that the underlying thrust is almost flat. We have inferred dips within the Neogene sediments. However, the sedimentary relationships will depend on whether earlier sediments were deposited in the footwall of an active range-front fault, in which case the units would thicken towards the range-front.

each flank (as in Fig. 7d). But the overall vergence of folding is in all cases to the west. This indicates that the eastward dipping faults which underlie the western margins of the folds are dominant. However, it would be difficult to see this without detailed field mapping. Drainage networks provide further information and are discussed below.

The Fosha (Fig. 6) and Sardar (Fig. 8) folds provide good examples. Each has a clear asymmetry to the drainage patterns that surround it. West of the folds there is no drainage incision, with westward flowing rivers forming active alluvial fans as they leave the folds. However, east of the folds, widespread incision continues for ~ 10 km into the Shotori mountains. This indicates that the region east of the folds is uplifting with respect to the region west of the folds, presumably on a fault that dips eastwards beneath the folds. The clearest example of this is the Sardar river (Figs 5d-e and 8a), which cuts a very narrow gorge up to 100 m deep. Sections drawn through the Fosha (Fig. 6c) and Sardar (Fig. 8c) folds indicate ~ 40 m of height difference of the alluvial surface across the fold. This fan surface can be traced through the folds (e.g. the light-coloured fan in Fig. 8a), implying ~ 40 m of uplift (and therefore incision) has occurred across the folds since the fan was deposited. The Sardar gorge leaves the Shotori mountain range ~ 40 m below a well preserved river terrace (Fig. 5f) that passes into the extensive gravel fans on the plain (Fig. 5g). The range front does not interrupt this terrace level, indicating that the range front fault has been inactive at the surface at least since the development of the uplifted terrace. This indicates a migration of activity away from the range front and is very similar to examples from the Tien Shan (Avouac *et al.* 1993) and Mongolia (Bayasgalan *et al.* 1999b) where activity is also inferred to have migrated away from the main range-front, presumably in response to stresses generated by topography.

Fig. 9 is a cartoon cross-section through the Sardar fold segment (see Fig. 8 for location). The proposed configuration is simple and

consistent with the geomorphology, earthquake source parameters and co-seismic ruptures. Slip on a gently east-dipping fault drives fold growth and secondary faulting in alluvial gravels west of the Shotori mountains. This implies a westward migration of activity at the surface. However, the Tabas faults probably interact with re-activated inherited structures of the Shotori mountains at mid to lower crustal levels (Berberian 1982). Right-lateral shear is present in both co-seismic ruptures and in strike-slip faults that cut alluvium and displace river systems along the western margin of the Shotori mountains (Fig. 10). A right-lateral component is also determined for the earthquakes in 1978, 1979 and 1980, and presumably relates to the role of the Tabas thrust in accommodating strike-slip motion at the end of the Nayband fault to the south, perhaps by local rotational deformation (Fig. 1c).

We conclude that all the major parts of this interpretation can be inferred directly from the landscape, illustrating that if we know what signs to look for, we can identify zones of active thrust faulting even if they have not experienced recent earthquake activity, and even if no discrete fault scarps are reported at the surface. Several authors have described the geomorphic expression of long-term fault-driven folding (Bayasgalan *et al.* 1999b; Keller *et al.* 1998; Oskin *et al.* 2000), the response of drainage systems and sedimentation to localised tectonic uplift (e.g. Burbank *et al.* 1996) and the forcing of surface deformation by discrete earthquake events (e.g. Berberian *et al.* 2001). By combining observations of seismicity, co-seismic surface deformation, and geomorphic indications of long-term folding and uplift we produce a simple and self-consistent picture of the faulting at Tabas.

4 FERDOWS

We have shown that indications of active faulting at Tabas are present in the landscape. We now use the observations made at Tabas to investigate two thrust earthquakes in 1968 near Ferdows (Fig. 1c).

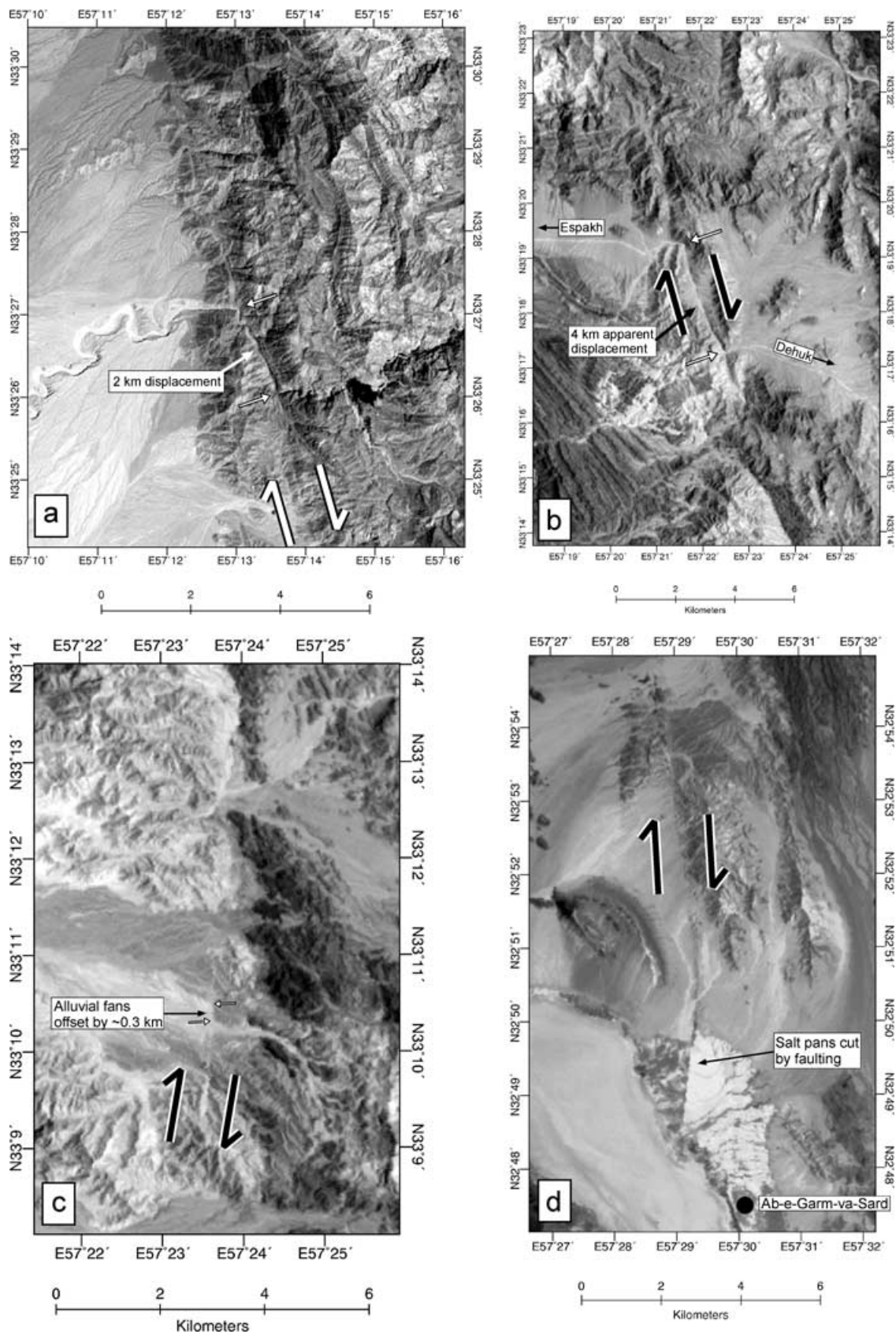


Figure 10. Right-lateral strike-slip faulting, displacing river courses and alluvium within the Shotori mountains. From north to south (see Fig. 2, for locations). (a) ASTER view of drainage displaced by ~2 km near Espakh. (b) 4 km displacement of alluvial gravels and drainage. The old Espakh-Dehuk road follows the displaced river channel. (c) ~300 m displacement of young alluvial fans. (d) The northern end of the Nayband fault at Ab-e-Garm-va-Sard. The faulting cuts young salt deposits in dry lake beds and continues north along the western margin of the Shotori mountains.

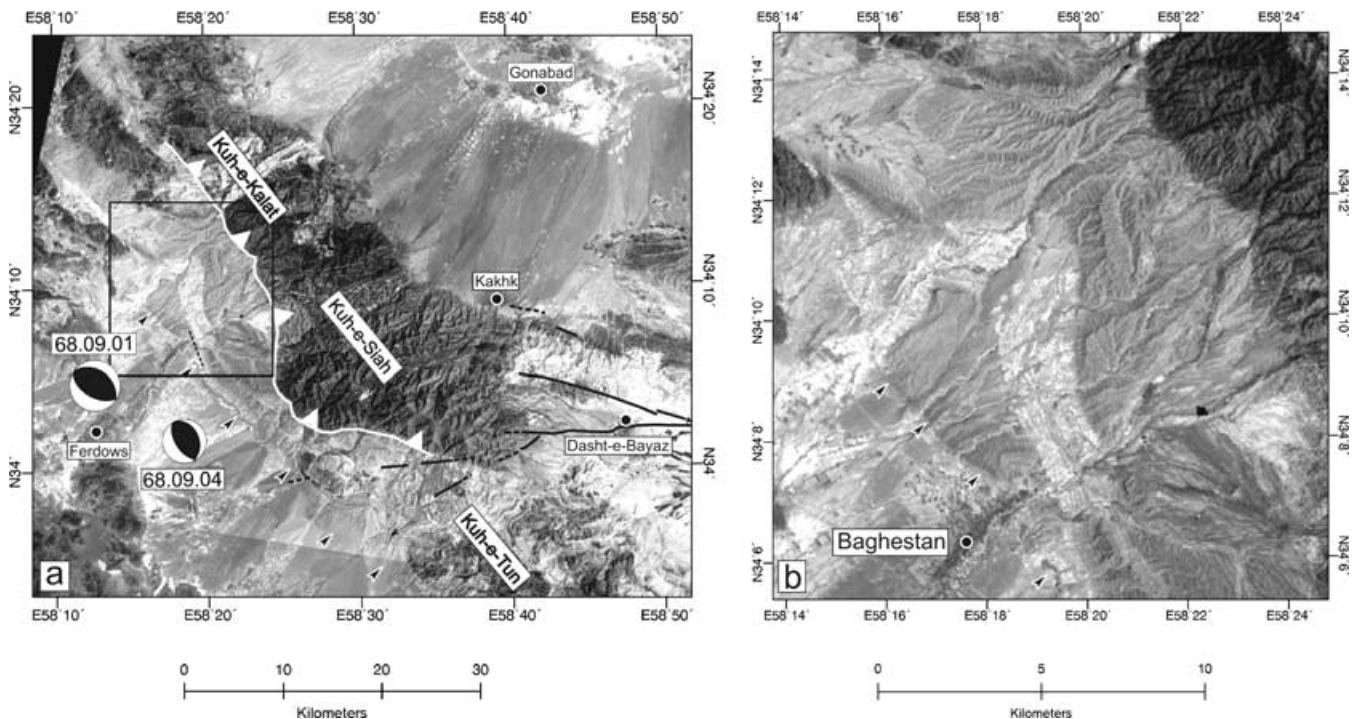


Figure 11. (a) LANDSAT TM mosaic of the Ferdows region. Thrust faulting is inferred beneath the region of uplifted and tilted alluvium and river terraces (marked by black arrows). This is some 10 km from the present-day mountain range front, which is defined by an older thrust fault (marked as a white toothed line). Possible co-seismic surface ruptures (Ambraseys & Melville 1982) are shown as a black dotted line northeast of Ferdows. Right-lateral surface ruptures of the Dasht-e-Bayaz earthquake (Ambraseys & Tchalenko 1969) are marked as solid black lines. Fault plane solutions for the two Ferdows earthquakes (see Fig. 14) are in black. Epicentres are from the catalogue of Engdahl *et al.* (1998) and may be inaccurate by up to 15 km for events after 1970, and by more for earlier events. Box shows location of Fig. 11(b). (b) LANDSAT TM close-up of uplifted Quaternary terraces and alluvium and incised river channels east of Ferdows. The NE–SW trending grey and white lithologies are eastward dipping Neogene conglomerates and marls.

Neither produced surface faulting that was recognised at the time, nor were active faults identified in their epicentral region prior to the earthquakes. Using the landscape, we can relate the earthquakes to surface uplift in the epicentral region, which in turn is related to slip on an underlying thrust fault. We also identify signs of recent faulting in the field.

4.1 Geological and tectonic setting

Ferdows (Fig. 11a) lies on an alluvial plain west of the Kuh-e-Kalat, Kuh-e-Siah and Kuh-e-Tun mountain ranges. These are composed of heavily deformed Jurassic sediments, with small amounts of older limestones and Tertiary volcanics (dacitic lava and pyroclastics) and granites. The western margin of these mountains is bounded by a substantial thrust fault (marked as white toothed line on Fig. 11a), which can easily be traced in the field, as the distinctive blue fault gouge is quarried as a roofing material (Fig. 12a). Drainage from the Kuh-e-Kalat range flows westwards towards one of several clay and salt flats. These depressions constitute local base-levels and are internally draining. Quaternary alluvial deposits shed from the western margin of the Kuh-e-Kalat range cover an eastward-dipping sequence of Neogene marls and conglomerates (Eftekhar-Nezhad & Ruttner 1970). The alluvial and fluvial deposits are slightly folded and show prominent drainage incision for a distance of ~10 km west of the range front (Fig. 11b). We infer below that this incision reflects surface uplift and folding above a thrust fault (black arrows on Fig. 11a, shown in detail on Fig. 11b).

4.2 Recent seismic and long-term deformation at Ferdows

Satellite imagery shows a clear western limit of river incision and uplift of alluvium and river terraces along a line trending $\sim 320^\circ$ (Fig. 11) that is also clear in the field (Fig. 12b–c). River incision continues east of this line into the Kuh-e-Kalat mountains. The dips of river terrace deposits steepen towards the southwestern flank of the fold (Fig. 12c). Unconformable relationships between older (steeper) and overlying gravels were seen in several localities (Fig. 12c–d). This asymmetry of folding and drainage incision is reminiscent of Tabas and shows that the surface folding is related to an eastward dipping structure at depth. Direct evidence of faulting is shown in Fig. 12(g)–(h), where uplifted river terraces that are near-horizontal 200 m NE of the frontal scarp are tilted to $\sim 70^\circ$ over less than 5 m distance at the scarp itself, caused by collapse of the upthrown block where co-seismic faulting has reached the surface (Fig. 13). Similar effects were seen after the 1980 El Asnam earthquake (Yielding *et al.* 1981). It is probable that faulting was parallel to bedding in underlying Neogene marls, which are exposed nearby and dip $\sim 30^\circ$ E (Fig. 12f). The overall wavelength of the surface uplift is ~ 15 km, and we therefore expect the underlying fault to extend to a similar depth. This is supported by the source parameters of the 1968 earthquakes (see below).

The Neogene deposits that outcrop beneath fluvial and alluvial gravels dip eastwards right across the folded region, even where the overlying gravels have been folded over to steep westward dips (Fig. 12e–f). This implies that the eastward dip of the Neogene beds pre-dates the present-day folding and represents deposition in the footwall of the older, more easterly thrust fault (the white toothed

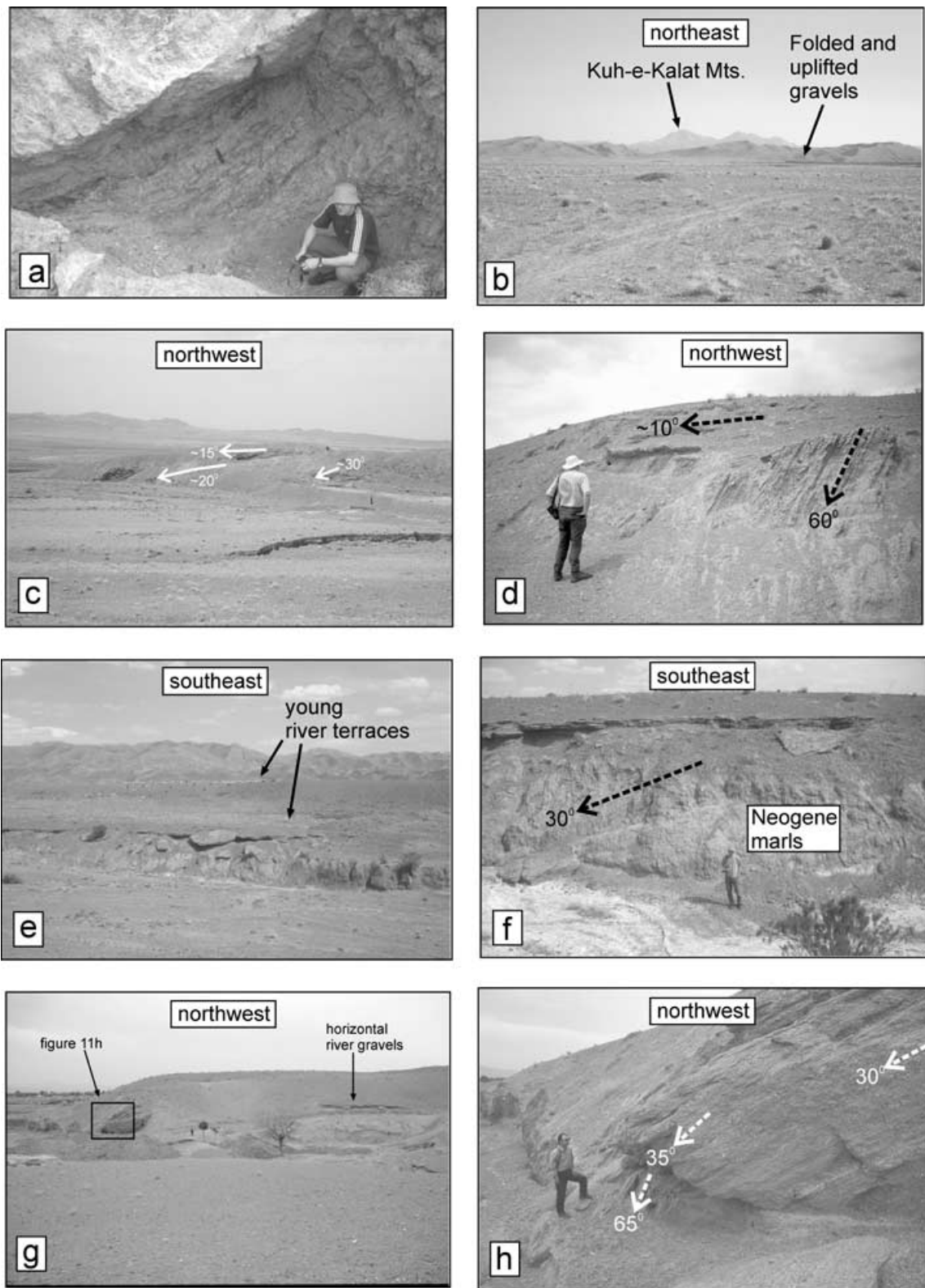


Figure 12. (a) Photograph of exposed fault-zone in Quarry at Amrudkhan ($34^{\circ} 14' .014N$ $58^{\circ} 21' .336E$). The fault gouge dips $\sim 40^{\circ}$ E. (b) View looking eastwards at uplifted fluvial and alluvial deposits that are incised by rivers. The western break in incision is sharp. The bed-rock mountains of Kuh-e-Kalat are ~ 15 km away. (c) Looking NW at the wall of a river cutting at $34^{\circ} 07' .801N$ $58^{\circ} 17' .499E$, bedding in alluvial gravels show growth in the flank of the fold. Individual beds steepen westwards and also truncate underlying steeper beds. (d) Unconformable relationships in alluvial gravels at $34^{\circ} 08' .949N$ $58^{\circ} 16' .592E$. (e) Looking southeast across an incised river at $34^{\circ} 06' .53N$ $58^{\circ} 19' .036E$. Two uplifted terrace levels can be seen. (f) Close-up of the river cutting in Fig. 12(e). Young river terraces are almost horizontal, but underlying Neogene deposits dip $\sim 30^{\circ}$ E. (g) Collapsed fold flank at $34^{\circ} 06' .368N$ $58^{\circ} 18' .843E$, ~ 100 m southwest of Fig. 12(f). Uplifted river gravels are horizontal in the right of the picture, but steepen rapidly in the left. (h) Gravel beds steepen rapidly in less than 10 m. This may be showing collapse of the fold flank where faulting has reached almost to the surface.

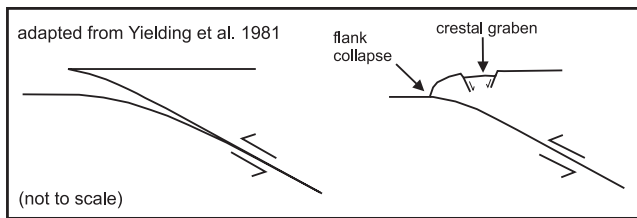


Figure 13. Cartoon showing how the relationships seen in Fig. 12(g-h) may have formed. The main rupture was on a plane dipping at $\sim 30^\circ$. Near the surface, the fault shallows out and causes the flank of the fold to collapse. Minor normal faulting might be expected at the crest of the fold.

line in Fig. 11a). A westward migration of active faulting would account for the prominent zone of folding and uplift of alluvial and river terrace material between the frontal scarp and the main mountain front (Fig. 11). This interpretation is similar to that shown in Fig. 9 for Tabas. If the eastward-dipping Neogene deposits were deposited in the footwall of the range-front fault when it was active,

we would expect the beds to thicken eastwards, but we do not know if this is the case.

Long-period *P* and *SH* body waves were inverted to obtain the earthquake source parameters using the same method as for Tabas. The two solutions are shown in Fig. 14 and Table 2. They are similar, both showing thrust motion on planes dipping 34 and 37° NE. and with strike directions close to the $\sim 320^\circ$ trend of the folds described above. The epicentres of the 1968.09.01 and 1968.09.04 Ferdows earthquakes relocated by Engdahl *et al.* (1998) are all situated to the SW of Baghestan and apparently in the footwall of the fault inferred along the frontal scarp. No surface deformation is apparent at these epicentral locations. Possible co-seismic ruptures were reported east of Bagestan, within the fold described above (Jackson & Fitch 1979; Ambraseys & Melville 1982) but were not visited at the time by reliable observers. Furthermore, the epicentres are expected to be offset from their true position by at least 10 km (Berberian 1979b). As the Ferdows fold is the only known Quaternary structure that is obviously active within 10 to 15 km of the reported epicentres, and where possible co-seismic ruptures were developed, it seems likely that the Ferdows

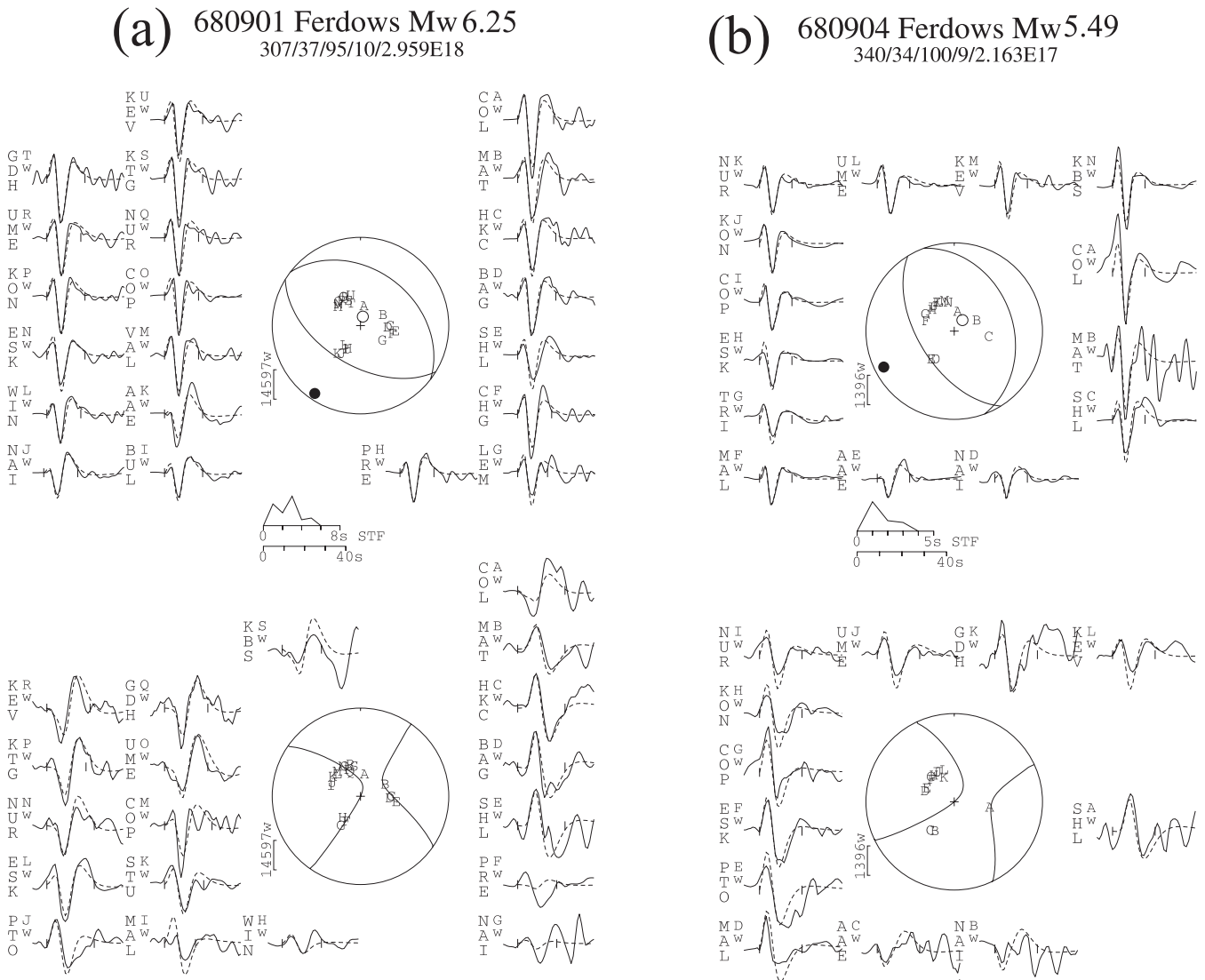


Figure 14. Final inversion results for the two Ferdows earthquakes of (a) 1968 September 01, and (b) 1968 September 04.

earthquakes occurred on faults beneath this folding, though we cannot prove this.

In conclusion, even though we have very little knowledge of the ground deformations associated with the 1968 Ferdows earthquakes, we can again use observations of the geomorphology to show long-term folding to the east of Ferdows. The asymmetry of the folding implies that it overlies an eastward dipping fault that projects to the surface near the frontal scarp at Baghestan. Once again, indications of folding, linked to active earthquake-generating thrust faulting are there in the landscape and are clear in satellite imagery. The present-day activity is again seen to have migrated away from the mountain range-fronts and is expressed at the surface as folding in alluvial gravels.

5 IMPLICATIONS FOR EARTHQUAKE HAZARD IN EASTERN IRAN AND ELSEWHERE

The towns of Tabas and Ferdows were not identified as zones at high risk from seismic activity until destructive earthquakes occurred on faults near them. In Tabas, over 20,000 people died and many settlements were destroyed. The identification of active blind thrusting is obviously important for estimating seismic hazard. The image interpretation and field data presented in this paper show numerous indications of long-term fold growth that is related to movement on eastward-dipping thrust faults at depth. Such indications cannot show conclusively that a structure is seismically active as movements may occur aseismically (as we suspect is the case in the growth seen on the Shahdad blind thrust in central Iran, described in Berberian *et al.* (2001). Also, we can only say that growth has occurred in the recent past, and without the use of palaeoseismological or exposure dating techniques on uplifted surfaces we cannot be precise about the exact age and duration of uplift (unlike, for example, at Wheeler Ridge in California or central Otago in New Zealand; Keller *et al.* 1998; Jackson *et al.* 2002). However, study of the geomorphology can highlight the potential for earthquakes to occur on a given structure (e.g. Oskin *et al.* 2000), and allow identification of similar surface features to those found at Tabas and Ferdows, even without guidance from previous recorded seismicity.

6 CONCLUSIONS

Indications of active, fault-driven folding and drainage incision are present in the landscape in both Tabas and Ferdows. Modern satellite imagery enhances our ability to see the sometimes subtle patterns of uplift and drainage incision. If we had known how to interpret these signs, the potential for destructive earthquakes in these regions could have been properly assessed. This is an important lesson for seismic hazard evaluation, not only in Iran, but also other regions of active continental deformation where thrust faulting is known to occur, but where the faulting itself does not produce clear, discrete scarps at the surface. Studies of this sort can also shed light on the long-term development and evolution of the fault zones.

ACKNOWLEDGMENTS

We would like to thank M.T. Khorehei and M. Qorashi of the Geological Survey of Iran in Tehran for their continued support of our work and for enabling us to visit the region in several field seasons. M. Talebian and Dan McKenzie made valuable contributions during the fieldwork. We thank M. Berberian for making available detailed maps of the 1978 co-seismic ruptures, and E. Keller and J. Shaw for helpful reviews. A digital elevation model was produced with

the kind assistance of B. Parsons and T. Wright at the University of Oxford. RW was supported by a NERC studentship. This work was supported by the NERC Centre for the Observation and Modelling of Earthquakes and Tectonics (COMET). This is Cambridge Earth Science Contribution No. 7076.

REFERENCES

- Ambraseys, N.N. & Tchalenko, J.S., 1969. The Dasht-e-Bayaz (Iran) earthquake of August 31, 1968: A field report, *Bull. Seism. Soc. Am.*, **59**, 1751–1792.
- Ambraseys, N.N. & Melville, C.P., 1982. A history of Persian earthquakes, Cambridge University Press, Cambridge.
- Avouac, J.P., Tapponnier, P., Bai, M., You, H. & Wang, G., 1993. Active thrusting and folding along the northern Tien Shan and Late Cenozoic rotation of the Tarim relative to Dzungaria and Kazakhstan, *J. geophys. Res.*, **98**, 6755–6804.
- Bayasgalan, A., Jackson, J., Ritz, J-F. & Carretier, S., 1999. Field examples of strike-slip fault terminations in Mongolia and their tectonic significance, *Tectonics*, **18**, 394–411.
- Bayasgalan, A., Jackson, J., Ritz, J-F. & Carretier, S., 1999b. 'Forebergs,' flower structures, and the development of large intracontinental strike-slip faults: the Gurvan Bogd fault system in Mongolia, *J. struc. geol.*, **21**, 1285–1302.
- Berberian, M., 1979a. Earthquake faulting and bedding thrust associated with the Tabas-e-Golshan (Iran) earthquake of September 16, 1978, *Bull. seism. Soc. Am.*, **69**, 1861–1887.
- Berberian, M., 1979b. Evaluation of instrumental and relocated epicentres of Iranian earthquakes, *Geophys. J. R. astr. Soc.*, **58**, 625–630.
- Berberian, M., Asudeh, I., Bilham, R.G., Scholz, C.H. & Soufleris, C., 1979. Mechanism of the main shock and the aftershock study of the Tabas-e-Golshan (Iran) earthquake of September 16, 1978: A preliminary report, *Bull. seism. Soc. Am.*, **69**, 1851–1859.
- Berberian, M., 1982. Aftershock tectonics of the 1978 Tabas-e-Golshan (Iran) earthquake sequence: a documented active 'thin- and thick-skinned tectonic' case, *Geophys. J. R. astr. Soc.*, **68**, 499–530.
- Berberian, M., Jackson, J.A., Qorashi, M., Talebian, M., Khatib, M.M. & Priestley, K., 2000. The 1994 Sefidabeh earthquakes in eastern Iran: blind thrusting and bedding-plane slip on a growing anticline, and active tectonics of the Sistan suture zone, *Geophys. J. Int.*, **142**, 283–299.
- Berberian, M. *et al.*, 2001. The 1998 March 14 Fandoqa earthquake (M_w 6.6) in Kerman province, southeast Iran: re-rupture of the 1981 Sirch earthquake fault, triggering of slip on adjacent thrusts and the active tectonics of the Gowk fault zone, *Geophys. J. Int.*, **146**, 371–398.
- Boudiaf, A., Ritz, J-F. & Philip, H., 1998. Drainage diversions as evidence of propagating active faults: example of the El Asnam and Thenia faults, Algeria, *Terra Nova*, **10**, 236–244.
- Bullard, T.F. & Lettis, W.R., 1993. Quaternary fold deformation associated with blind thrust faulting, Los Angeles basin, California, *J. geophys. Res.*, **98**, 8349–8369.
- Burbank, D., Meigs, A. & Brozovic, N., 1996. Interactions of growing folds and coeval depositional systems, *Basin Research*, **8**, 199–223.
- Eftekhari-Nezhad, J. & Ruttner, A., 1970. Geological Survey of Iran Geological quadrangle map of Iran No. J6 (Ferdows sheet), scale 1:250,000.
- Engdahl, E.R., van der Hilst, R. & Buland, R., 1998. Global teleseismic earthquake relocation with improved travel times and procedures for depth determination, *Bull. seism. Soc. Am.*, **88**, 722–743.
- Hauksson, E. & Jones, L.M., 1989. The 1987 Whittier Narrows earthquake sequence in Los Angeles, southern California: Seismological and tectonic analysis, *J. geophys. Res.*, **94**, 9569–9589.
- Hauksson, E., Jones, L.M. & Hutton, K., 1995. The 1994 Northridge earthquake sequence in California: Seismological and tectonic aspects, *J. geophys. Res.*, **100**, 12 335–12 355.
- Jackson, J.A. & Fitch, T.J., 1979. Seismotectonic implications of relocated aftershock sequences in Iran and Turkey, *Geophys. J. R. astr. Soc.*, **57**, 209–229.
- Jackson, J.A., Haines, J. & Holt, W., 1995. The accommodation of Arabia-Eurasia plate convergence in Iran, *J. geophys. Res.*, **100**, 15 205–15 219.

- Jackson, J.A., Norris, R. & Youngson, J., 1996. The structural evolution of active fault and fold systems in central Otago, New Zealand: evidence revealed by drainage patterns, *J. struc. geol.*, **18**, 217–234.
- Jackson, J.A., Ritz, J.-F., Siame, L., Raisbeck, G., Yiou, F., Norris, R., Youngson, J. & Bennett, E., 2002. Fault growth and landscape development rates in Otago, New Zealand, using in situ cosmogenic ¹⁰Be, *Earth planet. Sci. Lett.*, **195**, 185–193.
- Keller, E.A., Zepeda, R.L., Rockwell, T.K., Ku, T.L. & Dinklage, W.S., 1998. Active tectonics at Wheeler Ridge, southern San Joaquin Valley, California, *Bull. geol. soc. Am.*, **110**, 298–310.
- Lamb, S.H. & Vella, P., 1987. The last million years of deformation in part of the New Zealand plate-boundary zone, *J. struc. geol.*, **9**, 877–891.
- McCaffrey, R. & Abers, G., 1988. SYN3: a program for inversion of teleseismic body waveforms on microcomputers, *Air Force Geophysical Laboratory Technical Report, AFGL-TR-88-0099*, Hanscomb Air Force Base, MA.
- McCaffrey, R., Zwick, P. & Abers, G., 1991. SYN4 Program, *LASPEI Software Library*, **3**, 81–166.
- Meyer, B., Tapponnier, P., Bourjot, L., Metivier, F., Gaudemar, Y., Peltzer, G., Shunmin, G. & Zhitai, C., 1998. Crustal thickening in Gansu-Qinghai, lithospheric mantle subduction, and oblique, strike-slip controlled growth of the Tibet plateau, *Geophys. J. Int.*, **135**, 1–47.
- Nabelek, J., 1984. Determination of earthquake source parameters from inversion of body waves, *PhD thesis*, MIT, Cambridge MA.
- Niazi, M. & Kanamori, H., 1981. Source parameters of 1978 Tabas and 1979 Qainat, Iran, earthquakes from long-period surface waves, *Bull. seism. Soc. Am.*, **71**, 1201–1213.
- Oskin, M., Sieh, K., Rockwell, T., Miller, G., Guptill, P., Curtis, M., McArdle, S. & Elliot, P., 2000. Active parasitic folds on the Elysian Park anticline: Implications for seismic hazard in central Los Angeles, California, *Bull. geol. soc. Am.*, **112**, 693–707.
- Shoja-Taheri, J. & Anderson, J.G., 1988. The 1978 Tabas, Iran, earthquake: an interpretation of the strong motion records, *Bull. seism. Soc. Am.*, **78**, 142–171.
- Scholz, C., 1982. Scaling laws for large earthquakes: consequences for physical models, *Bull. seism. Soc. Am.*, **72**, 1–14.
- Silver, P.G. & Jordan, T.H., 1983. Total-moment spectra of fourteen large earthquakes, *J. geophys. Res.*, **88**, 3273–3293.
- Stöcklin, J., Eftekhari-Nezhad, J. & Hushmand-zadeh, A., 1965. Geology of the Shotori Range (Tabas area, East Iran), *Geological survey of Iran, Report No. 3*.
- Taymaz, T., Jackson, J. & McKenzie, D., 1991. Active tectonics of the north and central Aegean Sea, *Geophys. J. Int.*, **106**, 433–490.
- Yielding, G., Jackson, J.A., King, G.C.P., Sinval, H., Vita-Finzi, C. & Wood, R.M., 1981. Relations between surface deformation, fault geometry, seismicity, and rupture characteristics during the El Asnam (Algeria) earthquake of 10 October 1980, *Earth planet. Sci. Lett.*, **56**, 287–304.
- Zwick, P., McCaffrey, R. & Abers, G., 1995. MT5 Program, *LASPEI Software Library* 4.